Research Article | Vol. 24, No. 22 | 31 Oct 2016 | OPTICS EXPRESS 24907

Optics EXPRESS

Dispersion of nondegenerate nonlinear refraction in semiconductors

Peng Zhao,[1] Matthew Reichert,[1,2] David J. Hagan,[1,3] and Eric W. Van Stryland[1,3,*]

[1]*CREOL, College of Optics and Photonics, University of Central Florida, Orlando, FL 32816, USA*
[2]*Current address: Department of Electrical Engineering, Princeton University, Princeton, NJ 08455, USA*
[3]*Department of Physics, University of Central Florida, Orlando, FL 32816, USA*
[*]*ewvs@creol.ucf.edu*

Abstract: We use our recently developed beam-deflection technique to measure the dispersion of the nondegenerate nonlinear refraction (NLR) of direct-gap semiconductors. The magnitude and sign of the NLR coefficient $n_2(\omega_a; \omega_b)$ are determined over a broad spectral range for different values of nondegeneracy. In the extremely nondegenerate case, $n_2(\omega_a; \omega_b)$ is positively enhanced near the two-photon absorption (2PA) edge and is significantly larger than its degenerate counterpart, suggesting applications for nondegenerate all-optical switching. At higher photon energies within the 2PA regime, $n_2(\omega_a; \omega_b)$ switches sign to negative over a narrow wavelength range. This strong anomalous nonlinear dispersion provides large phase modulation of a femtosecond pulse with bandwidth centered near the zero-crossing frequency. The measured nondegenerate dispersion closely follows our earlier predictions based on nonlinear Kramers-Kronig relations [Sheik-Bahae et. al, IEEE J. Quant. Electron. 30, 249 (1994)].

OCIS codes: (190.3270) Kerr effect; (300.6470) Spectroscopy, semiconductors; (190.7110) Ultrafast nonlinear optics; (130.4815) Optical switching devices.

References and links

1. J. A. Armstrong, N. Bloembergen, J. Ducuing, and P. S. Pershan, "Interactions between Light Waves in a Nonlinear Dielectric," Phys. Rev. **127**(6), 1918–1939 (1962).
2. R. W. Boyd, *Nonlinear Optics*, 3 ed. (Academic Press, 2008).
3. G. I. Stegeman and R. A. Stegeman, *Nonlinear Optics: Phenomena, Materials and Devices*, Wiley Series in Pure and Applied Optics (John Wiley & Sons, Inc., 2012).
4. D. E. Spence, P. N. Kean, and W. Sibbett, "60-fsec pulse generation from a self-mode-locked Ti:sapphire laser," Opt. Lett. **16**(1), 42–44 (1991).
5. E. W. Van Stryland, Y. Y. Wu, D. J. Hagan, M. J. Soileau, and K. Mansour, "Optical limiting with semiconductors," J. Opt. Soc. Am. B **5**(9), 1980–1988 (1988).
6. E. W. Van Stryland, H. Vanherzeele, M. A. Woodall, M. J. Soileau, A. L. Smirl, S. Guha, and T. F. Boggess, "Two Photon Absorption, Nonlinear Refraction, And Optical Limiting In Semiconductors," Opt. Eng. **24**(4), 244613 (1985).
7. H. S. Eisenberg, Y. Silberberg, R. Morandotti, A. R. Boyd, and J. S. Aitchison, "Discrete Spatial Optical Solitons in Waveguide Arrays," Phys. Rev. Lett. **81**(16), 3383–3386 (1998).
8. G. I. Stegeman and M. Segev, "Optical Spatial Solitons and Their Interactions: Universality and Diversity," Science **286**(5444), 1518–1523 (1999).
9. V. R. Almeida, C. A. Barrios, R. R. Panepucci, and M. Lipson, "All-optical control of light on a silicon chip," Nature **431**(7012), 1081–1084 (2004).
10. D. C. Hutchings, J. S. Aitchison, and C. N. Ironside, "All-optical switching based on nondegenerate phase shifts from a cascaded second-order nonlinearity," Opt. Lett. **18**(10), 793–795 (1993).
11. C. Koos, P. Vorreau, T. Vallaitis, P. Dumon, W. Bogaerts, R. Baets, B. Esembeson, I. Biaggio, T. Michinobu, F. Diederich, W. Freude, and J. Leuthold, "All-optical high-speed signal processing with silicon-organic hybrid slot waveguides," Nat. Photonics **3**(4), 216–219 (2009).
12. G. I. Stegeman and E. M. Wright, "All-optical waveguide switching," Opt. Quantum Electron. **22**(2), 95–122 (1990).
13. G. I. Stegeman, E. M. Wright, N. Finlayson, R. Zanoni, and C. T. Seaton, "Third order nonlinear integrated optics," J. Lightwave Technol. **6**(6), 953–970 (1988).

#270561 http://dx.doi.org/10.1364/OE.24.024907
Journal © 2016 Received 14 Jul 2016; accepted 11 Oct 2016; published 17 Oct 2016

Optics EXPRESS

14. P. K. Wa, J. E. Sitch, N. J. Mason, J. S. Roberts, and P. N. Robson, "All optical multiple-quantum-well waveguide switch," in *Electronics Letters* (Institution of Engineering and Technology, 1985), pp. 26–28.
15. A. Villeneuve, C. C. Yang, P. G. J. Wigley, G. I. Stegeman, J. S. Aitchison, and C. N. Ironside, "Ultrafast all-optical switching in semiconductor nonlinear directional couplers at half the band gap," Appl. Phys. Lett. **61**(2), 147–149 (1992).
16. S. Nakamura, K. Tajima, and Y. Sugimoto, "Experimental investigation on high- speed switching characteristics of a novel symmetric Mach–Zehnder all- optical switch," Appl. Phys. Lett. **65**(3), 283–285 (1994).
17. K. Nozaki, T. Tanabe, A. Shinya, S. Matsuo, T. Sato, H. Taniyama, and M. Notomi, "Sub-femtojoule all-optical switching using a photonic-crystal nanocavity," Nat. Photonics **4**(7), 477–483 (2010).
18. J. S. Pelc, K. Rivoire, S. Vo, C. Santori, D. A. Fattal, and R. G. Beausoleil, "Picosecond all-optical switching in hydrogenated amorphous silicon microring resonators," Opt. Express **22**(4), 3797–3810 (2014).
19. V. Van, T. A. Ibrahim, K. Ritter, P. P. Absil, F. G. Johnson, R. Grover, J. Goldhar, and P. T. Ho, "All-optical nonlinear switching in GaAs-AlGaAs microring resonators," IEEE Photonics Technol. Lett. **14**(1), 74–76 (2002).
20. D. C. Hutchings, M. Sheik-Bahae, D. J. Hagan, and E. W. Van Stryland, "Kramers-Krönig relations in nonlinear optics," Opt. Quantum Electron. **24**(1), 1–30 (1992).
21. M. Sheik-Bahae, "Nonlinear Optics of Bound Electrons in Solids," in *Nonlinear Optical Materials*, J. V. Moloney, ed. (Springer, 1998), pp. 205–224.
22. M. Sheik-Bahae, J. Wang, and E. W. V. Stryland, "Nondegenerate optical Kerr effect in semiconductors," IEEE J. Quantum Electron. **30**(2), 249–255 (1994).
23. M. Sheik-Bahae, D. C. Hutchings, D. J. Hagan, and E. W. Van Stryland, "Dispersion of bound electron nonlinear refraction in solids," IEEE J. Quantum Electron. **27**(6), 1296–1309 (1991).
24. C. Aversa, J. E. Sipe, M. Sheik-Bahae, and E. W. Van Stryland, "Third-order optical nonlinearities in semiconductors: The two-band model," Phys. Rev. B Condens. Matter **50**(24), 18073–18082 (1994).
25. M. Sheik-Bahae, A. A. Said, T.-H. Wei, D. J. Hagan, and E. W. Van Stryland, "Sensitive measurement of optical nonlinearities using a single beam," IEEE J. Quantum Electron. **26**(4), 760–769 (1990).
26. M. Balu, J. Hales, D. Hagan, and E. Van Stryland, "Dispersion of nonlinear refraction and two-photon absorption using a white-light continuum Z-scan," Opt. Express **13**(10), 3594–3599 (2005).
27. M. Balu, J. Hales, D. Hagan, and E. Van Stryland, "White-light continuum Z-scan technique for nonlinear materials characterization," Opt. Express **12**(16), 3820–3826 (2004).
28. D. C. Hutchings and B. S. Wherrett, "Theory of the dispersion of ultrafast nonlinear refraction in zinc-blende semiconductors below the band edge," Phys. Rev. B Condens. Matter **50**(7), 4622–4630 (1994).
29. D. A. Fishman, C. M. Cirloganu, S. Webster, L. A. Padilha, M. Monroe, D. J. Hagan, and E. W. Van Stryland, "Sensitive mid-infrared detection in wide-bandgap semiconductors using extreme non-degenerate two-photon absorption," Nat. Photonics **5**(9), 561–565 (2011).
30. H. S. Pattanaik, M. Reichert, D. J. Hagan, and E. W. Van Stryland, "Three-dimensional IR imaging with uncooled GaN photodiodes using nondegenerate two-photon absorption," Opt. Express **24**(2), 1196–1205 (2016).
31. M. Reichert, A. L. Smirl, G. Salamo, D. J. Hagan, and E. W. Van Stryland, "Observation of Nondegenerate Two-Photon Gain in GaAs," Phys. Rev. Lett. **117**(7), 073602 (2016).
32. C. M. Cirloganu, L. A. Padilha, D. A. Fishman, S. Webster, D. J. Hagan, and E. W. Van Stryland, "Extremely nondegenerate two-photon absorption in direct-gap semiconductors [Invited]," Opt. Express **19**(23), 22951–22960 (2011).
33. G. I. Stegeman, "Material figures of merit and implications to all-optical waveguide switching," in *OE/LASE'93: Optics, Electro-Optics, & Laser Applications in Science& Engineering*, (International Society for Optics and Photonics, 1993), pp. 75–89.
34. V. Mizrahi, M. A. Saifi, M. J. Andrejco, K. W. DeLong, and G. I. Stegeman, "Two-photon absorption as a limitation to all-optical switching," Opt. Lett. **14**(20), 1140–1142 (1989).
35. M. R. Ferdinandus, H. Hu, M. Reichert, D. J. Hagan, and E. W. Van Stryland, "Beam deflection measurement of time and polarization resolved ultrafast nonlinear refraction," Opt. Lett. **38**(18), 3518–3521 (2013).
36. P. Zhao, M. Reichert, T. R. Ensley, W. M. Shensky, A. G. Mott, D. J. Hagan, and E. W. Van Stryland, "Nonlinear refraction dynamics of solvents and gases," Proc. SPIE **9731**, 97310F (2016).
37. M. Reichert, H. Hu, M. R. Ferdinandus, M. Seidel, P. Zhao, T. R. Ensley, D. Peceli, J. M. Reed, D. A. Fishman, S. Webster, D. J. Hagan, and E. W. Van Stryland, "Temporal, spectral, and polarization dependence of the nonlinear optical response of carbon disulfide," Optica **1**(6), 436–445 (2014).
38. M. Reichert, P. Zhao, J. M. Reed, T. R. Ensley, D. J. Hagan, and E. W. Van Stryland, "Beam deflection measurement of bound-electronic and rotational nonlinear refraction in molecular gases," Opt. Express **23**(17), 22224–22237 (2015).
39. H. Shima and T. Nakayama, eds., *Higher Mathematics for Physics and Engineering* (Springer Science & Business Media, 2010).
40. E. W. Van Stryland, M. A. Woodall, H. Vanherzeele, and M. J. Soileau, "Energy band-gap dependence of two-photon absorption," Opt. Lett. **10**(10), 490–492 (1985).
41. J. A. Bolger, A. K. Kar, B. S. Wherrett, R. DeSalvo, D. C. Hutchings, and D. J. Hagan, "Nondegenerate two-photon absorption spectra of ZnSe, ZnS and ZnO," Opt. Commun. **97**(3-4), 203–209 (1993).

Optics EXPRESS

42. D. C. Hutchings and E. W. Van Stryland, "Nondegenerate two-photon absorption in zinc blende semiconductors," J. Opt. Soc. Am. B **9**(11), 2065–2074 (1992).
43. A. N. Naumov and A. M. Zheltikov, "Frequency–time and time–space mappings with broadband and supercontinuum chirped pulses in coherent wave mixing and pump–probe techniques," Appl. Phys. B **77**(2-3), 369–376 (2003).
44. D. R. Solli, J. Chou, and B. Jalali, "Amplified wavelength-time transformation for real-time spectroscopy," Nat. Photonics **2**(1), 48–51 (2008).
45. J. Chou, Y. Han, and B. Jalali, "Time-wavelength spectroscopy for chemical sensing," IEEE Photonics Technol. Lett. **16**(4), 1140–1142 (2004).
46. P. V. Kelkar, F. Coppinger, A. S. Bhushan, and B. Jalali, "Time-domain optical sensing," Electron. Lett. **35**(19), 1661–1662 (1999).
47. D. Milam, "Review and Assessment of Measured Values of the Nonlinear Refractive-Index Coefficient of Fused Silica," Appl. Opt. **37**(3), 546–550 (1998).
48. R. A. Negres, J. M. Hales, A. Kobyakov, D. J. Hagan, and E. W. Van Stryland, "Experiment and analysis of two-photon absorption spectroscopy using a white-light continuum probe," IEEE J. Quantum Electron. **38**(9), 1205–1216 (2002).
49. A. E. Kaplan, "External self-focusing of light by a nonlinear layer," Radiophys. Quantum Electron. **12**(6), 692–696 (1969).
50. M. Reichert, P. Zhao, H. S. Pattanaik, D. J. Hagan, and E. W. Van Stryland, "Nondegenerate two- and three-photon nonlinearities in semiconductors," in *Ultrafast Bandgap Photonics*, Proc. SPIE **9835**, 98350A (2016).
51. M. Balu, L. A. Padilha, D. J. Hagan, E. W. Van Stryland, S. Yao, K. Belfield, S. Zheng, S. Barlow, and S. Marder, "Broadband Z-scan characterization using a high-spectral-irradiance, high-quality supercontinuum," J. Opt. Soc. Am. B **25**(2), 159–165 (2008).
52. I. H. Malitson, "Interspecimen Comparison of the Refractive Index of Fused Silica*,†," J. Opt. Soc. Am. **55**(10), 1205–1209 (1965).
53. W. L. Bond, "Measurement of the Refractive Indices of Several Crystals," J. Appl. Phys. **36**(5), 1674–1677 (1965).
54. B. Tatian, "Fitting refractive-index data with the Sellmeier dispersion formula," Appl. Opt. **23**(24), 4477–4485 (1984).
55. M. S. Gomez, J. M. Guerra, and F. Vilches, "Weighted nonlinear regression analysis of a Sellmeier expansion: comparison of several nonlinear fits of CdS dispersion," Appl. Opt. **24**(8), 1147–1150 (1985).
56. T. R. Ensley, H. Hu, M. Reichert, M. R. Ferdinandus, D. Peceli, J. M. Hales, J. W. Perry, Z. Li, S.-H. Jang, A. K. Y. Jen, S. R. Marder, D. J. Hagan, and E. W. Van Stryland, "Quasi-three-level model applied to measured spectra of nonlinear absorption and refraction in organic molecules," J. Opt. Soc. Am. B **33**(4), 780–796 (2016).
57. K. DeLong, K. Rochford, and G. Stegeman, "Effect of two-photon absorption on all-optical guided-wave devices," Appl. Phys. Lett. **55**(18), 1823–1825 (1989).

1. Introduction

In semiconductors, bound-electronic nonlinear refraction (NLR), also known as the optical Kerr effect, is one of the dominant optical nonlinearities in the sub-gap regime, resulting in a refractive index change, Δn, directly proportional to the irradiance with coefficient n_2 [1–3]. Owing to the fast response of bound valence electrons, the Kerr effect has been exploited for various ultrafast applications including Kerr-lens mode locking [4], optical limiting [5,6] and soliton propagation [7,8]. Another application of n_2 of semiconductors is all-optical switching (AOS) [9–14], particularly in waveguide geometries such as nonlinear directional couplers [15], Mach-Zehnder interferometers [10,16] or resonant cavities [17–19], in which the transmission of the signal beam can be modulated by a control beam. Precise knowledge of the magnitude, sign, and dispersion of n_2 of semiconductors is needed for the design and prediction of AOS devices. In general, NLR is related to nonlinear absorption (NLA) via a Kramers-Kronig (KK) transformation of the nondegenerate (ND) NLA spectrum [20,21]. This theory has been extensively used for prediction of n_2 of various solids [22–24]. For a single beam at frequency ω, Z-scan measurements of this nonlinear refractive index, denoted by $n_2(\omega; \omega)$, have shown excellent agreement with theoretical predictions [25–28]. However, the ND-NLR, namely the refractive index change at frequency ω_a due to the presence of a beam at frequency ω_b, of coefficient $n_2(\omega_a; \omega_b)$, is much less explored, particularly for the extremely nondegenerate case (i.e. $\hbar\omega_a \gg \hbar\omega_b$) and for spectral regions where 2PA is present.

We have observed orders of magnitude enhancement of two-photon absorption (2PA), of coefficient $\alpha_2(\omega_a; \omega_b)$, using extremely nondegenerate photon pairs. Such enhancement has

Optics EXPRESS

been utilized in applications including mid-infrared pulse detection [29], 3D IR imaging [30] and observation of two-photon gain [31]. Linked by KK relations, the nondegenerate enhancement of 2PA translates into enhancement of $n_2(\omega_a; \omega_b)$ [22,32], which suggests the use of semiconductors for applications such as nondegenerate AOS. The enhanced $n_2(\omega_a; \omega_b)$ lowers the switching energy required for various device geometries [33]. Traditional AOS devices with degenerate or nearly degenerate signal and control beams operate best below or near half the bandgap energy, E_g, to avoid loss from 2PA [15,19,34]. This excludes certain materials to be used for efficient Kerr effect based AOS at wavelengths of interest such as the telecommunication band. Nondegenerate operating schemes for AOS have the potential to overcome such limitations, as it tailors the nonlinearities, and, in principle, allows any signal wavelength below the bandgap to be used without the presence of 2PA. In the extremely nondegenerate case, the theory predicts that when $\hbar\omega_a \to E_g$, the positively enhanced $n_2(\omega_a; \omega_b)$ becomes anomalously dispersive and rapidly switches sign from a large positive value to a large negative value over a very narrow spectral range, i.e., ~10 nm [32]. This rapid anomalous nonlinear dispersion provides a large modulation for a femtosecond pulse with bandwidth centered near the zero crossing frequency. This may enable other applications such as nonlinear pulse shaping. However, it should be noted that the ND-2PA is also greatly enhanced in this same spectral region.

In this paper, we perform an extensive experimental study of the dispersion of ND-NLR for three direct-gap semiconductors (ZnO, ZnSe, and CdS) using our recently developed beam-deflection (BD) technique [35]. BD is a highly sensitive excite-probe technique capable of simultaneously measuring the absolute magnitude, sign, and temporal dynamics of both NLR and NLA. We previously applied BD to measure the nonlinearity of fused silica [35], the response functions of various liquid solvents [36,37] and NLR transients of molecular gases [38]. Here, using very different excitation and probe wavelengths, the dispersion of the ND-NLR is measured over the sub-gap region, along with ND-2PA or nondegenerate three-photon absorption (ND-3PA). We observe the resonance enhancement of NLR and the rapid anomalous dispersion near the bandgap. The results are compared to theoretical predictions from the KK transformation of [22,23]. We also define a nondegenerate figure of merit (FOM) for AOS in both ND-2PA and ND-3PA regimes and compare theory and experiment showing potential advantages with respect to the degenerate case.

2. Theory

As a consequence of causality in any linear system, a dispersion relation governs the real and imaginary parts of the frequency-domain complex response function via Hilbert transform pairs [39]. In optical systems, this principle results in the Kramers-Kronig transformation, which relates the real and imagery parts of the linear susceptibility [20]. To include nonlinear effects, we introduce nondegenerate perturbations on the refractive index $\Delta n = 2n_2(\omega_a; \omega_b)I_b$ and absorption $\Delta\alpha = 2\alpha_{NL}(\omega_a; \omega_b)I_b$ due to the presence of an excitation optical field at frequency ω_b with irradiance I_b. After subtracting the linear components and dividing out I_b, we derive the KK transformation that relates ND-NLR with ND-NLA [22,23].

$$n_2(\omega_a;\omega_b) = \frac{c}{\pi} P\int_0^\infty \frac{\alpha_{NL}(\omega';\omega_b)}{\omega'^2 - \omega_a^2} d\omega', \tag{1}$$

where α_{NL} is the total NLA coefficient, c is the speed of light and P donates the Cauchy principle value of the complex integral. Note that the degenerate NLR $n_2(\omega_b; \omega_b)$ can be evaluated by performing the integral and then taking $\omega_a = \omega_b$. As discussed in [20–24], this method of using KK with the ND-NLA linearizes the problem since the change in absorption is linear in the probe irradiance.

In semiconductors, the major physical mechanisms of $\alpha_{NL}(\omega_a; \omega_b)$ consist of 2PA, electronic Raman and the optical (AC) Stark effect, which together can be viewed as the

Optics EXPRESS

overall change of absorption of a material due to the presence of an excitation beam at ω_b. As graphically illustrated in Fig. 1(a), ND-2PA describes simultaneous absorption of both photons of frequency ω_a and ω_b, which requires $\hbar\omega_a + \hbar\omega_b \geq E_g$. Stimulated Raman scattering leads to simultaneous absorption and emission of photons at ω_a and ω_b, respectively, where $|\hbar\omega_a - \hbar\omega_b| \geq E_g$ is required. The optical Stark effect, also referred to as virtual band blocking [23], can be viewed as saturation of linear absorption for $\hbar\omega_a \geq E_g$, caused by virtual carriers generated by a strong beam at ω_b. The nondegenerate NLA spectra of 2PA, Raman and AC Stark effect were formulated previously based on a two-parabolic band model using perturbation theory [22,23], from which the nondegenerate $n_2(\omega_a; \omega_b)$ dispersion is calculated via the KK transformation resulting in;

$$n_2(\omega_a;\omega_b) = \frac{\hbar cK}{2}\frac{\sqrt{E_p}}{n_a n_b E_g^4} G_2\left(\frac{\hbar\omega_a}{E_g};\frac{\hbar\omega_b}{E_g}\right), \tag{2}$$

where E_p is the Kane energy parameter, and n_a and n_b are the linear refractive indices at the respective frequencies. G_2 is the dimensionless dispersion function as explicitly defined for each corresponding NLA mechanism in [22,23]. K is a material-dependent parameter, which is ~3100 cm GW^{-1} $eV^{5/2}$ from an experimental best fit in [6,40], but may vary by a factor of ~2 from one semiconductor to another due to the simplicity in the assumption of the band structure [6,22,23]. This simple theory results in a generality, making it possible to predict NLR of various solids given the bandgap, Kane energy, linear index and optical frequencies.

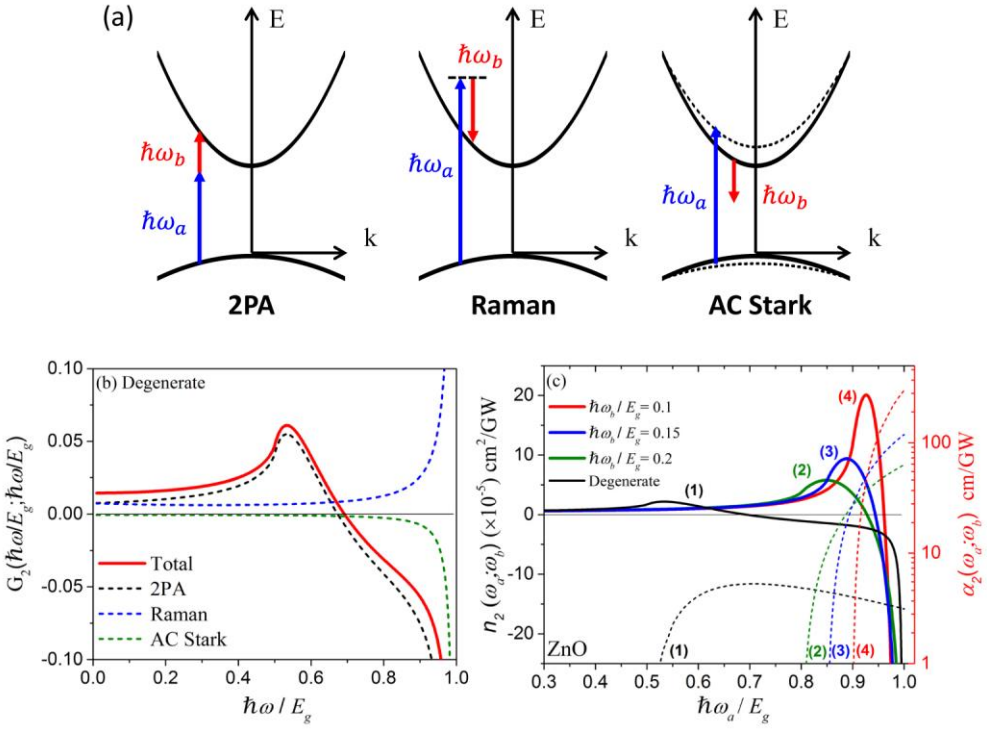

Fig. 1. (a) Illustrations of nondegenerate NLA processes contributing to NLR in the sub-gap regime; (b) calculated degenerate NLR dispersion function G_2 with total contribution (solid line) decomposed into 2PA, Raman and AC Stark contributions (dashed lines) [22]; (c) calculated ND-NLR (solid lines) and ND-2PA (dashed lines) coefficients of ZnO with excitation photon energy $\hbar\omega_b$ of 20% (2), 15% (3) and 10% (4) of the bandgap, as compared to the degenerate case (1).

Optics EXPRESS

In Fig. 1(b), the dispersion function G_2 for degenerate ($\omega_a = \omega_b$) NLR is calculated from [22,23], which is independent of materials and therefore represents the universal nonlinear dispersion of direct-gap semiconductors. The total G_2 is decomposed into contributions from 2PA, Raman, and AC Stark effect. Of these, 2PA contributes the most in the spectral region well below the bandgap, which grows from low frequencies to a maximum near $E_g/2$ (onset of 2PA) and then becomes anomalously dispersive and ultimately turns negative as $\hbar\omega$ approaches the bandgap.

With highly nondegenerate photon pairs, the two-photon transition rate is greatly enhanced due to intermediate-state resonance enhancement (ISRE) of the small photon energy with the intraband self-transition and the larger photon energy with the interband transition [32,41,42]. This directly results in the enhancement of 2PA, e.g., 270 × enhancement measured in ZnSe using photons with a ratio of energies of 12 [32]. Based on the ND-2PA spectrum derived from a two-band model, the ND-NLR dispersion can be calculated via a KK transformation from Eq. (2). Figure 1(c) shows the calculated $n_2(\omega_a; \omega_b)$ and $\alpha_2(\omega_a; \omega_b)$ of ZnO by varying $\hbar\omega_a$ from 0 to E_g with the excitation photon energy, $\hbar\omega_b$, fixed at 20% (λ_b = 1.9 μm), 15% (2.5 μm) and 10% (3.8 μm) of the bandgap. The degenerate spectra of $n_2(\omega_a; \omega_a)$ and $\alpha_2(\omega_a; \omega_a)$ are also shown for comparison. Linked by KK relation, $n_2(\omega_a; \omega_b)$ is positive for low ω_a and grows to a maximum near the ND-2PA resonance ($\hbar\omega_a = E_g - \hbar\omega_b$). Then $n_2(\omega_a; \omega_b)$ becomes anomalously dispersive and ultimately switches to negative as $\hbar\omega_a$ approaches the bandgap. Associated with ISRE of ND-2PA, $n_2(\omega_a; \omega_b)$ is positively enhanced near $\hbar\omega_a = E_g - \hbar\omega_b$, and the increase of nondegeneracy ($\hbar\omega_a/\hbar\omega_b$) results in larger enhancement. In the extremely nondegenerate case, with $\hbar\omega_b$ only ~10% of E_g, the maximum $n_2(\omega_a; \omega_b)$ is enhanced by ~30 × over its zero-frequency limit ($\hbar\omega_a$ = 0), and ~9 × larger than the maximum for the degenerate case. However, the nondegenerate NLR changes sign and is not as enhanced as the ND-2PA. Also, the anomalous dispersion near the bandgap becomes very steep for extremely ND-NLR, and $n_2(\omega_a; \omega_b)$ can switch sign over a very narrow spectral range. For example, with $\hbar\omega_b = 0.1E_g$, $n_2(\omega_a; \omega_b)$ changes from 11×10^{-5} cm^2/GW to -11×10^{-5} cm^2/GW by varying $\hbar\omega_a$ from 3.1 eV (400 nm) to 3.2 eV (388 nm). Picosecond pulses with narrow bandwidth might be required to resolve such rapid anomalous dispersion experimentally. However, one can also directly observe this nonlinear dispersion using a linearly chirped femtosecond pulse with its bandwidth centered near the zero crossing frequency of $n_2(\omega_a; \omega_b)$. This is similar to time-wavelength spectroscopy [43–46], as discussed in detail in Section 4.

3. Nondegenerate beam deflection

To experimentally measure ND-NLR of semiconductors, we utilize our recently developed beam-deflection technique [35–38]. BD is an excite-probe technique where we use fs pulses along with a temporal delay line, as shown in Fig. 2(a). The strong excitation pulse at ω_b creates an index change $\Delta n(\mathbf{r}) = 2n_2(\omega_a; \omega_b)I_b(\mathbf{r})$ that follows its Gaussian spatial irradiance distribution, shown in Fig. 2(b). The probe pulse at ω_a is focused to a spot size ~3-5 × smaller than that of the excitation beam and is spatially displaced to the Gaussian wings off the excitation's center where the index gradient is nearly constant and maximized. This deflects the probe by a small angle which is measured using a position sensitive segmented detector by taking the difference of the energy falling on the left and right halves, $\Delta E = Eleft - Eright$, and normalizing to the total energy E. The BD signal, $\Delta E/E$, is directly proportional to $n_2(\omega_a; \omega_b)$, and the transmission change in E is proportional to the NLA (here 2PA). By choosing different wavelengths of excitation and probe, BD measures the magnitudes and signs of both nondegenerate NLR and NLA as well as their temporal dynamics. These measurements make possible the determination of the material FOM.

We use a commercial Ti:sapphire laser system (Coherent Legend Elite Duo HE +) producing ~12 mJ, ~40 fs (FWHM) pulses at a 1 kHz repetition rate to pump an optical

Optics EXPRESS

parametric generator/amplifier (TOPAS-800, Light Conversion) to generate the excitation pulses from the idler beam at a wavelength of λ_b = 2.3 μm with ~150 nm bandwidth (FWHM), which is then focused to a beam waist of w_b = 210 μm (HW1/e^{2}M) at the sample. To obtain the probe pulses with wavelength tunability, another beam from the Ti:sapphire laser system is focused into a 1 cm quartz cuvette filled with water to produce a white-light continuum (WLC), which is then spectrally filtered using narrow bandpass interference filters (10-25 nm, FWHM) to select wavelengths in the range of λ_a = 430-750 nm. The measured beam waist of the probe for different wavelengths at the sample varies from w_a = 30-50 μm (HW1/e^{2}M). The beam crossing angle is kept < 2°. The linear polarization of the excitation and probe beams was maintained using polarizers and for most experiments was set to be parallel to each other; however, we also used crossed polarizations for some cases where noted. The deflection of the probe induced by the excitation pulse is detected using a quad-segmented Si photodiode (OSI QD50-0-SD) placed in the far field after the sample. Both ΔE and E are detected via a lock-in amplifier (Stanford Research Systems, SR830) at the 285 Hz modulation frequency of an optical chopper in the excitation beam. While this technique is in principle absolutely calibrated [35,37], the relative errors between different wavelengths and samples can be reduced by comparing to a standard reference. In this work, all BD measurements of the semiconductors studied were conducted relative to the results obtained from a 1 mm thick fused silica sample using $n_2 = 2.5 \times 10^{-16}$ cm^2/W [47].

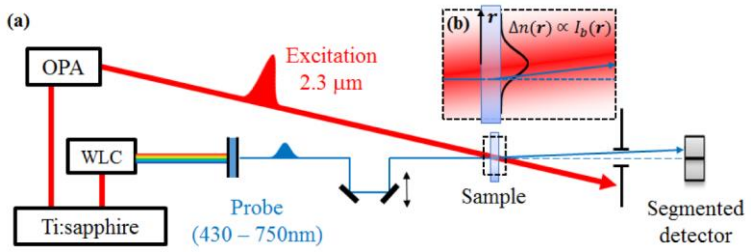

Fig. 2. (a) Illustration of the nondegenerate BD experiment [35]; (b) spatial irradiance distribution of the excitation beam (red) and overlapping geometry with the probe beam (blue) at the sample plane.

The bound-electronic nonlinearity leads to a nearly instantaneous response for NLR, which only occurs when the excitation and probe pulses are temporally overlapped within the sample. In extremely nondegenerate experiments, significant group velocity mismatch (GVM) between excitation and probe pulses causes temporal walk-off within the sample. Following Negres et. al. [48], we have developed a methodology to account for GVM in the BD analysis [37], which analytically solves the electric field distribution of the probe at the rear surface of the sample including the effects of NLR induced by the excitation. This allows us to fit BD data and extract $n_2(\omega_a; \omega_b)$. To do this, we first define the probe electric field to be $\mathbf{E}_a(\mathbf{r}, z, t) = \tfrac{1}{2}E_a(\mathbf{r}, z, t)\exp[i(k_a z - \omega_a t)]\hat{\mathbf{e}} + c.c.$, where E_a is the complex field amplitude, $\mathbf{r}$ is the radial vector, $k_a = n_a\omega_a/c$ is the wave number, and $\hat{\mathbf{e}}$ is the unit vector in the probe field direction. Within the slowly-varying-envelope approximation [2,3], the nonlinear wave equation is derived to describe the evolution of a weak probe propagating through the sample in z;

$$i\left(\frac{\partial E_a}{\partial z}+\frac{n_{g,a}}{c}\frac{\partial E_a}{\partial t}\right)=-\left\{2k_{0,a}n_2(\omega_a;\omega_b)+i\alpha_2(\omega_a;\omega_b)+i\frac{3}{2}\alpha_3(\omega_a;\omega_b,\omega_b)I_b(t)\right\}I_b(t)E_a, \quad (3)$$

where $n_{g,a}$ is the group index of the sample at the probe frequency ω_a. Here, the group velocity dispersion (GVD) and linear absorption are neglected. The thin sample approximation is also applied (external self-action [49]), meaning the sample thickness L is less than the Rayleigh ranges of both beams and the nonlinear induced phase distortion does

Optics EXPRESS

not propagate within the sample to produce irradiance changes on either beam. In our experiments with fixed $\hbar\omega_b$, $\alpha_2(\omega_a; \omega_b)$ is nonzero only if $\hbar\omega_a \geq (E_g - \hbar\omega_b)$. For $(E_g - \hbar\omega_b) > \hbar\omega_a \geq (E_g - 2\hbar\omega_b)$, the dominant NLA becomes ND-3PA, of coefficient $\alpha_3(\omega_a; \omega_b, \omega_b)$, with two photons from the excitation and one from the probe absorbed [50]. Assuming temporally Gaussian pulses following [37,48,50] and analytically solving for E_a at the back surface of the sample, we obtain:

$$E_a = E_{0,a} \exp\left(-\frac{(T - T_d - \rho)^2}{2(\tau_a / \tau_b)^2} + \frac{i}{\rho}\int_{T-\rho}^{T} \left\{ 2k_a n_2(\omega_a;\omega_b) + i\alpha_2(\omega_a;\omega_b) + i\frac{3}{2}\alpha_3(\omega_a;\omega_b,\omega_b) I_b(T) \right\} L I_b(T)\, dT \right), \quad (4)$$

where $E_{0,a}$ is the input probe field, $T = (t - n_{g,a}z/c)/\tau_b$ and T_d are the normalized time and delayin the frame of the excitation pulse, respectively, and τ_a and τ_b are pulse durations (HW1/eM) for probe and excitation, respectively. $\rho = (n_{g,a} - n_{g,b})L/(c\tau_b)$ is the GVM parameter, related to the temporal walk-off between excitation and probe pulses. Treating $n_2(\omega_a; \omega_b)$, $\alpha_2(\omega_a; \omega_b)$ and $\alpha_3(\omega_a; \omega_b, \omega_b)$ as invariant w.r.t. T, Eq. (4) can be further simplified to:

$$E_a = E_{0,a} \exp\left(-\frac{(T - T_d - \rho)^2}{2(\tau_a / \tau_b)^2} + \frac{i\sqrt{\pi}}{2\rho} \left\{ 2k_a n_2(\omega_a;\omega_b) + i\alpha_2(\omega_a;\omega_b) \right\} L I_{b,0} \left[\mathrm{erf}(T) - \mathrm{erf}(T - \rho) \right] \right.$$
$$\left. - \frac{3\sqrt{2\pi}}{8\rho} \alpha_3 L I_{b,0}^2 \left[\mathrm{erf}\left(\sqrt{2}T\right) - \mathrm{erf}\left(\sqrt{2}(T - \rho)\right) \right] \right). \quad (5)$$

The probe field at the detector can be calculated by numerically propagating E_a from Eq. (5) via Fresnel diffraction. Then ΔE and E are calculated by spatial and temporal integration of the probe irradiance profile at the detector, $I_a(\mathbf{r},t) = c\varepsilon_0|E_a(\mathbf{r},t)|^2/2$, which we fit to the experimental results to extract both nondegenerate NLR and NLA coefficients.

4. Results

Examples of measured BD signals ($\Delta E/E$) with fits are shown in Fig. 3(a), where ZnO, ZnSe, and CdS, along with a 1 mm thick fused silica sample, are measured under identical beam overlapping geometries with excitation ($\hbar\omega_b$ = 0.54 eV) and filtered WLC probe ($\hbar\omega_a$ = 1.9 eV). The respective beam radii are 210 μm and 35 μm. For fused silica, the GVM between excitation and probe pulses is negligible (ρ = 0.03 [52]), therefore $\Delta E/E$ simply follows the cross correlation of the two pulses. For semiconductor samples, GVM becomes a significant factor in interpreting the measured signals. Particularly in ZnSe and CdS, the temporal walk-off between excitation and probe within the sample results in a broadened $\Delta E/E$ towards negative delays where the probe comes prior to excitation but travels at a slower group velocity such that the faster excitation pulse catches up and walks through the probe over a distance less than L. The corresponding fits (solid lines) for each material take into account GVM using Eqs. (4, 5) where ρ = 3.7, 8.9 and 10.2 for ZnO [53], ZnSe [54], and CdS [55], respectively.

The measured dispersion of $n_2(\omega_a; \omega_b)$ for ZnO, ZnSe, and CdS is shown in Fig. 3(b-d) as red circles along with the theoretical calculations for both nondegenerate (red curve) and degenerate (black curve) cases. Errors in $n_2(\omega_a; \omega_b)$ are mainly from irradiance uncertainties as well as experimental noise in $\Delta E/E$, and those in $\hbar\omega_a/E_g$ originate from the bandwidth of the probe. In the measurements of ZnO, shown in Fig. 3(b), $\hbar\omega_b$ is fixed to ~16% of the bandgap, and the WLC probe is filtered at several wavelengths from 750 nm to 440 nm to map out the dispersion of $n_2(\omega_a; \omega_b)$. With $\hbar\omega_a/E_g < 0.68$ (λ_a > 600 nm), both 2PA and 3PA are not possible, since $\hbar\omega_a + 2\hbar\omega_b < E_g$, and no NLA is observed, giving values of $n_2(\omega_a; \omega_b)$ close to the zero-frequency limit. For $\hbar\omega_a/E_g$ = 0.69 and 0.72 (570 nm and 550 nm), ND-3PA occurs, and we measure $n_2(\omega_a; \omega_b)$ along with $\alpha_3(\omega_a; \omega_b, \omega_b)$. Significantly larger $n_2(\omega_a; \omega_b)$ is measured in the 2PA spectral region of $\hbar\omega_a/E_g$ = 0.82 – 0.90 (λ_a = 480 – 440 nm) owing to

Optics EXPRESS

the ISRE. Near the onset of 2PA (i.e., at λ_a = 480 nm), $n_2(\omega_a; \omega_b)$ is measured ~6 × larger than the degenerate n_2 (black squares) at 1.06 μm measured via Z-scan near its zero-frequency limit [23]. The greatest nondegenerate enhancement in ZnO is measured at λ_a = 440 nm, where $n_2(\omega_a; \omega_b)$ is more than one order-of-magnitude larger than the degenerate n_2 (black squares) at 1.06 μm measured via Z-scan near its zero-frequency limit [23] and ~3 × larger than the maximum of the calculated degenerate n_2. But it should be noted that at the wavelength where $n_2(\omega_a; \omega_b)$ reaches its maximum enhancement, ND-2PA is also greatly enhanced. Using K = 2400 cm GW^{-1} eV$^{5/2}$ in Eq. (2), gives good agreement with the measured ND-NLR. Additionally, the dependence of $n_2(\omega_a; \omega_b)$ on the polarization of the probe with respect to that of the excitation is also investigated for selected probe wavelengths. For λ_a = 550 and 600 nm, we measure that with perpendicularly polarized waves, $n_2(\omega_a; \omega_b)$ becomes 3.2 × and 2.7 × smaller respectively than for the parallel polarization case.

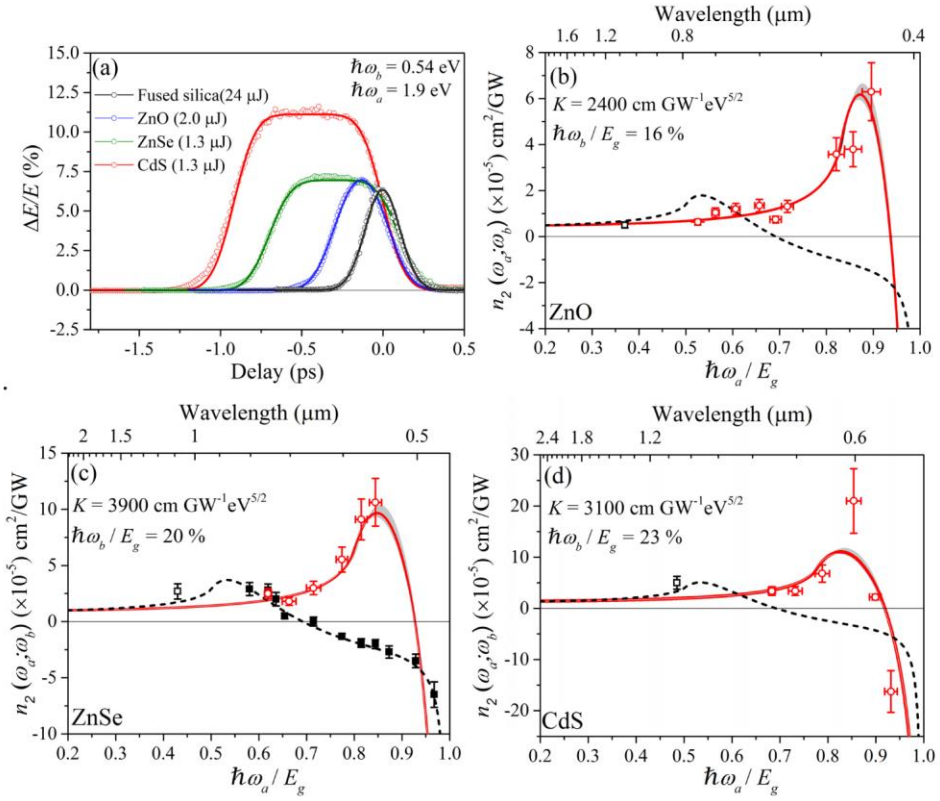

Fig. 3. (a) Examples of measured BD signals (circles) from ZnO, ZnSe, CdS, and fused silica, along with fits (lines) using Eqs. (3-5) considering GVM; Measured $n_2(\omega_a; \omega_b)$ dispersion (red circles) of (b) ZnO, (c) ZnSe, and (d) CdS, compared to theoretical calculations for nondegenerate (solid lines) and degenerate (dashed lines) n_2 using Eq. (2); Shaded region represents errors from the bandwidth of the excitation pulse; degenerate n_2 data is from [23] (open squares) and [51] (black squares).

For ZnSe, where $\hbar\omega_b$ ~20% of the bandgap, the increase of $n_2(\omega_a; \omega_b)$ is also observed as $\hbar\omega_a$ increases towards the 2PA resonance as shown in Fig. 3(c). For longer wavelengths (λ_a = 750 – 600 nm), ND-NLR is accompanied by ND-3PA. The data of degenerate n_2 dispersion (black squares) of ZnSe is taken from previous measurements using WLC Z-scan [51] for comparison. A remarkable agreement is found between theoretical calculations and experimental results from both BD and WLC Z-scan measurements when using the same K = 3900 cm GW^{-1} eV$^{5/2}$, indicating the consistency of the theory in both degenerate and

Optics EXPRESS

nondegenerate cases. This K value is similar to the previously reported K = ~4000 as the experimental best fit for ZnSe [22,23]. For λ_a = 600 and 750 nm, with perpendicularly polarized waves, $n_2(\omega_a; \omega_b)$ is measured to be 3.7 × and 2.4 × smaller respectively than the values measured with parallel polarizations. Note that the theoretical model assuming a two-parabolic band structure cannot account for this effect [22], but these ratios may be used to compare to the theory considering a more realistic band structure such as Kane's model [42,50].

As shown in Fig. 3(d), $n_2(\omega_a; \omega_b)$ of CdS is measured with $\hbar\omega_b$ ~23% of the bandgap. Besides the nondegenerate enhancement of n_2, the anomalous dispersion after the maximum, as well as the associated sign change, are also resolved with a probe wavelength very close to the bandgap (λ_a = 570 nm and 550nm). Particularly at λ_a = 570 nm near the zero-crossing frequency, a small value of n_2 (2.2 × 10^{-5} cm^2/GW) is measured in the presence of a large 2PA (13 cm/GW) background, indicating the excellent ability of BD for separately measuring NLR and NLA. Such a separation would be very difficult using other techniques, including Z-scan. All the measured nondegenerate NLR and NLA coefficients for ZnO, ZnSe and CdS are summarized in Table 1.

Table 1. Measured nondegenerate NLR and NLA coefficients for semiconductors with λ_b = 2.3 μm[a]

λ_a (nm)	$n_2(\omega_a; \omega_b)$ (10^{-5} cm^2/GW)			$\alpha_2(\omega_a; \omega_b)$ (cm/GW)			$\alpha_3(\omega_a; \omega_b, \omega_b)$ (10^{-3} cm^3/GW^2)		
	ZnO	ZnSe	CdS	ZnO	ZnSe	CdS	ZnO	ZnSe	CdS
440	6.3 ± 1.4			2.7 ± 0.6					
460	3.8 ± 0.9			0.5 ± 0.11					
480	3.6 ± 0.8			0.3 ± 0.07					
550	1.3 ± 0.3	10.6 ± 2.5	–16.3 ± 4		12.5 ± 2.8	28.8 ± 6.5	1.6 ± 0.4		
570	0.7 ± 0.15	9.1 ± 2.0	2.2 ± 0.6		3.1 ± 0.7	13.2 ± 3.0	< 0.8		
600	1.4 ± 0.3	5.5 ± 1.2	21.0 ± 6.3			50.0 ± 16		63.8 ± 16.0	
650	1.2 ± 0.25	2.9 ± 0.6	6.8 ± 1.4					38.0 ± 9.5	87.6 ± 22
700	1.0 ± 0.22	1.8 ± 0.4	3.4 ± 0.75					25.8 ± 6.5	41 ± 10
750	0.6 ± 0.15	2.5 ± 0.6	3.5 ± 0.75					38.4 ± 9.6	21.7 ± 5.4

[a]E_g measured for ZnO, ZnSe, and CdS are 3.2 eV, 2.6 eV and 2.4 eV, respectively.

Limited by the large bandwidth of femtosecond pulses, the frequency resolution is insufficient to directly measure the absolute value of n_2 near the bandgap in the extremely nondegenerate case (e.g. ZnO in Fig. 3(b)), as the theory predicts a rapid anomalous nonlinear dispersion followed by a sign change in a very narrow spectral range. Here we utilize a methodology similar to time-wavelength spectroscopy [43–46] to resolve this strongly dispersive NLR. In ZnO measurements with the same excitation of 2.3 μm, the WLC probe is filtered at a center wavelength of 430 nm to 10 nm (FWHM) bandwidth, which covers the zero-crossing frequency of $n_2(\omega_a; \omega_b)$ predicted by theory (422 nm). Higher and lower frequency components will see a negative and positive n_2, respectively, as shown in the inset of Fig. 4(a). In this experiment, the probe pulse is assumed to be linearly up-chirped, with lower frequencies arriving before higher frequencies, and the pulsewidth τ_a is determined to be ~500 fs from the cross-correlation in fused silica using the same BD setup. As shown in Fig. 4(b), the measured $\Delta E/E$ of ZnO is greatly different from the signals shown in Fig. 3(a), where the dispersion of $n_2(\omega_a; \omega_b)$ over the bandwidth of the probe is negligible. Around zero delay, the excitation temporally overlaps the rising edge of the probe pulse (lower frequency) at the front surface of the sample, giving a positive signal. A negative signal is observed at a delay of ~– 2.5 ps, where the excitation pulse overlaps with the falling edge of the probe (higher frequency) at the back surface of the sample. For delays in between, the excitation and probe completely walk through each other within the sample, giving an averaged small positive signal from all frequency components.

Optics EXPRESS

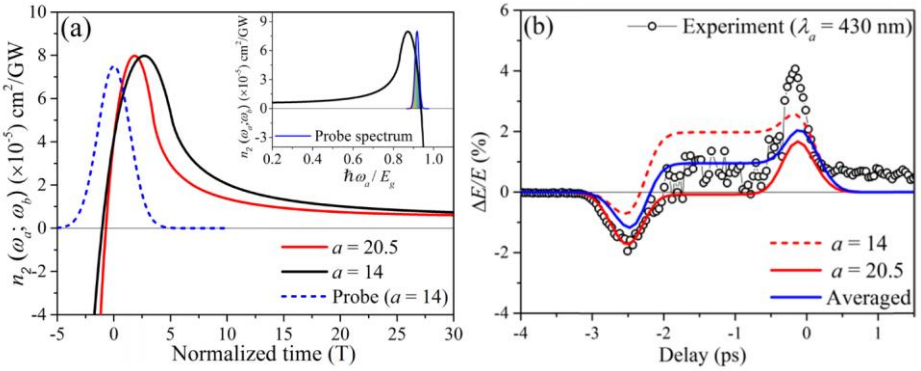

Fig. 4. (a) Converted $n_2(T)$ assuming linear chirp at the front (black) and back (red) surface of the sample compared to the initial probe pulsewidth (blue dashed). Inset is the theoretical $n_2(\omega_a; \omega_b)$ dispersion (black solid) of ZnO (same as Fig. 3(b)) relative to the probe bandwidth (blue solid) at λ_a = 430 nm. (b) measured $\Delta E/E$ (black circles), compared to theoretical predictions based on chirping conditions at the front (red dashed) and back (red solid) surface of the sample along with the averaged curve (blue solid).

To investigate this transient NLR quantitatively, the $n_2(\omega_a; \omega_b)$ dispersion is converted to a time-domain quantity via the instantaneous probe frequency, which is defined as

$$\omega_a(t) = \omega_{0,a} - \frac{2at}{\tau_G^2}, \tag{6}$$

where $\omega_{0,a}$ is the carrier frequency of the probe (here at 430 nm), τ_G is the pulsewidth of the probe field (HW$^1/_e$M), a is the chirping parameter, which is estimated as 14 for the initial input pulse based on the measured pulsewidth and spectrum. Due to GVD, the probe pulse is chirped further upon propagating through sample, which gives a = 20.5 at the back surface of sample, as calculated using the linear dispersion from [53]. $n_2(T)$ is calculated by substituting Eq. (6) into Eq. (2), which is plotted in Fig. 4(a) for the two different chirps at the front (red dashed) and back (red solid) surface of the sample, where the temporal profile of the probe (blue dashed) is also plotted for comparison. Clearly, Eq. (5) is not applicable for predicting $\Delta E/E$ in this experiment because $n_2(\omega_a; \omega_b)$ in Eq. (4) cannot be assumed to be constant in the integral of T. But the variation of $\alpha_2(\omega_a; \omega_b)$ is negligible within the same spectral (temporal) range. For extremely ND-NLR, this anomalous dispersion is very steep within the instantaneous frequency (or temporal profile) of the probe, so that we can take a first-order approximation to obtain a linear dependence of n_2 on $\omega_a(t)$ (or T), giving $n_2(\omega_a; \omega_b) = n_2(T) = n_{2,0} + n_{2,1}T$. By substituting this into Eq. (4), the output probe field with ND-2PA becomes,

$$E_a = E_{0,a}\exp\left(-\frac{(T-T_d-\rho)^2}{2(\tau_a/\tau_b)^2} + \frac{i\sqrt{\pi}}{2\rho}\left(2k_a n_{2,0} + i\alpha_2\right)LI_{b,0}\left[\operatorname{erf}(T) - \operatorname{erf}(T-\rho)\right] + \frac{i}{2\rho}2k_a n_{2,1}LI_{b,0}\left(e^{-(T-\rho)^2} - e^{-T^2}\right)\right) \tag{7}$$

where $n_{2,0}$ and $n_{2,1}$ are derived from a linear fit of $n_2(T)$ at T = 0. Figure 4(b) shows theoretical predictions of $\Delta E/E$ calculated from Eq. (4) for an initial probe chirp of a = 14 (red dashed) and that after the sample of a = 20.5 (red solid). The averaged curve between the two cases (blue solid) leads to a better agreement of the shape of the NLR transients. Note an even better agreement can be achieved by varying $n_{2,0}$ and $n_{2,1}$ as fitting parameters. Therefore, we confirm the theoretical prediction of the anomalous dispersive sign switching of extremely

Optics EXPRESS

nondegenerate n_2 near the bandgap, which provides a large nonlinear modulation of a femtosecond pulse.

5. Nondegenerate FOM of AOS

Owing to the large enhancement of NLR, the nondegenerate operating scheme can be implemented into Kerr-effect based photonic devices such as AOS, where the signal beam, with $\hbar\omega_a$ close to the bandgap, can be modulated with an infrared control beam at $\hbar\omega_b$. With a larger $n_2(\omega_a; \omega_b)$, the switching irradiance of the control beam, I_{sw}, can be significantly reduced for a required nonlinear phase change $\Delta\phi = 2k_a n_2(\omega_a; \omega_b) I_{sw} L$. In practice, the nonlinear loss terms imposed by ND-2PA and ND-3PA should satisfy $2\alpha_2(\omega_a; \omega_b) I_{sw} L < 1$ and $3\alpha_3(\omega_a; \omega_b, \omega_b) I_{sw}^2 L < 1$, respectively [33], from which FOMs are defined by the absolute value of the ratio of $\Delta\phi$ and loss terms as

$$FOM_{2PA} = 2\left|\frac{\Delta\phi}{2\alpha_2(\omega_a;\omega_b) I_{sw} L}\right| = \frac{4\pi}{\lambda_a}\left|\frac{n_2(\omega_a;\omega_b)}{\alpha_2(\omega_a;\omega_b)}\right| \tag{8}$$

$$FOM_{3PA} = 2\left|\frac{\Delta\phi}{3\alpha_3(\omega_a;\omega_b,\omega_b) I_{sw}^2 L}\right| = \frac{8\pi}{3\lambda_a}\left|\frac{n_2(\omega_a;\omega_b)}{\alpha_3(\omega_a;\omega_b,\omega_b) I_{sw}}\right| \tag{9}$$

where a factor of 2 is added to be consistent with other definitions (i.e., $FOM_{2PA} = |\mathrm{Re}(\chi^{(3)})/\mathrm{Im}(\chi^{(3)})|$) [56]. For different AOS geometries, both FOMs need to be larger than 4π for a Mach-Zehnder (MZ) interferometer [33], 8π for a nonlinear directional coupler (NLDC) [21,23] and $2/\sqrt{3}$ for a Fabry-Perot (FP) filter [34,57]. Table 2 summarizes measured nondegenerate FOM_{2PA} and FOM_{3PA} for ZnO, ZnSe, and CdS based on the definitions of Eqs. (8) and (9). It should be noted that the most enhanced n_2, measured with a probe at 440 nm, 550 nm, and 600 nm in ZnO, ZnSe, and CdS respectively, do not result in the largest FOM. This is because in the spectral region where nondegenerate enhancement of NLR is maximized, the enhancement of 2PA is even larger, leading to a smaller FOM_{2PA} [32]. The largest FOM values measured in the 2PA spectral region are either near the onset of 2PA (i.e. 480 nm in ZnO and 570 nm in ZnSe) or near the bandgap with a negative n_2 (i.e. 550 nm in CdS).

As an example, Fig. 5 shows measured FOM_{2PA} and FOM_{3PA} of ZnSe for both degenerate and nondegenerate cases, along with theoretical curves calculated using Eq. (2) and $\alpha_2(\omega_a; \omega_b)$ spectra from the same two-band model [22,23]. The degenerate data (black squares) are calculated based on the experimental results of n_2 and α_2 from [51]. Within the 2PA region, $\hbar\omega_a/E_g > 0.5$, the degenerate FOM_{2PA} is too small to meet the criteria of all the AOS geometries, except $\hbar\omega_a/E_g > 0.9$ where loss from band-tail absorption increases. This essentially limits the operating wavelength of ZnSe for AOS to below half of the bandgap, $\lambda_a > 928$ nm. Such limitations may be overcome with nondegenerate enhancement of NLR. In agreement with theory, the nondegenerate FOM_{2PA} (red circles) near the onset of ND-2PA ($\hbar\omega_a/E_g$ ~81%) is measured to be ~7 × larger than the degenerate FOM_{2PA} at the same wavelength of $\lambda_a = 570$ nm. The improvement over the degenerate case can become even larger with higher nondegeneracy (e.g. ~50 × in ZnO at $\lambda_a = 480$ nm). For $0.6 < \hbar\omega_a/E_g < 0.8$, ND-3PA becomes the dominate loss mechanism in ZnSe as ND-2PA no longer occurs since $\hbar\omega_a + \hbar\omega_b < E_g$. Based on Eq. (9), FOM_{3PA} is inversely proportional to I_{sw}. In Fig. 5, nondegenerate FOM_{3PA} of ZnSe is calculated from the measured parameters in Table 2 using two different irradiances, $I_{sw} = 10$ GW/cm^2 (green triangles) and $I_{sw} = 1$ GW/cm^2 (blue stars), where the smaller I_{sw} results in significant improvement of FOM_{3PA} over the degenerate case

Optics EXPRESS

in the same spectral region (i.e. ~340 × at λ_a = 700 nm) and satisfies the criteria of all AOS geometries.

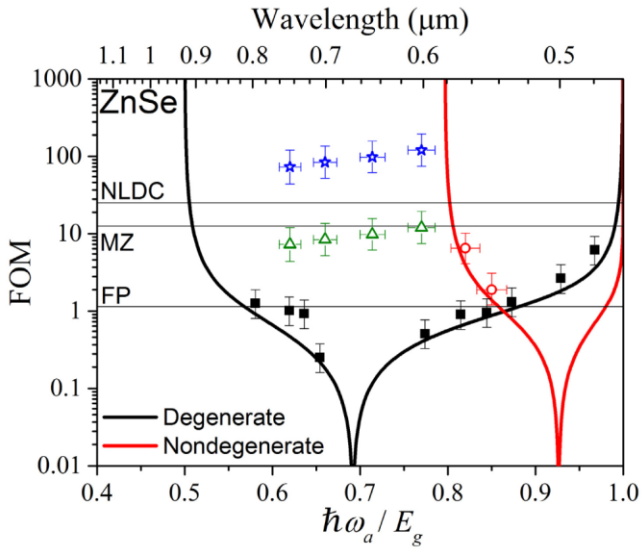

Fig. 5. Measured FOM of ZnSe in the presence of 2PA for degenerate (black squares) and nondegenerate (red circles) NLR, as compared to theory (solid lines) [22,23]; FOM in the presence of ND-3PA are based on I_{sw} = 10 GW/cm^2 (green triangles) and I_{sw} = 1 GW/cm^2 (blue stars). The degenerate data is from [51]. The minimum requirements for AOS geometries of a Mach-Zehnder (MZ) interferometer, nonlinear directional coupler (NLDC) and Fabry-Perot (FP) filter are included for comparison.

Table 2. Measured nondegenerate FOM in 2PA and 3PA spectral region [a, b]

λ_a (nm)	FOM		
	ZnO	ZnSe	CdS
440	6.7 (+ 3.8/-2.3)		
460	20.8 (+ 11.3/-7.6)		
480	31.4 (+ 18.7/-11.6)		
550	1238 (+ 793/-476)	1.9 (+ 1.2/-0.7)	1.3 (+ 0.7/-0.5)
570	>1286	6.5 (+ 3.7/-2.4)	0.37 (+ 0.23/-0.15)
600		120 (+ 75/-45)	0.88 (+ 0.8/-0.4)
650		98 (+ 60/-36)	100 (+ 61/-36)
700		84 (+ 52/-32)	99 (+ 61/-37)
750		73 (+ 47/-29)	180 (+ 111/-67)

[a]FOM is defined in Eqs. (8-9), where I_{sw} = 1 GW/cm^2 for FOM$_{3PA}$.
[b]The asymmetric error bars are calculated based on the upper and lower limits of n_2, α_2 and α_3 in **Table 1**.

6. Conclusions

We have presented experimental measurements on the dispersion of the nondegenerate nonlinear refraction of ZnO, ZnSe, and CdS using our recently developed beam-deflection technique. With various values of nondegeneracy, the ND-NLR coefficient $n_2(\omega_a; \omega_b)$ is measured over a broad spectral range, along with the corresponding ND-2PA and ND-3PA coefficients. To extract the values of these nonlinear coefficients, GVM has been taken into account in the analysis of the data. Using an excitation pulse at $\hbar\omega_b$ = 0.54 eV, a positively enhanced $n_2(\omega_a; \omega_b)$ is measured in all direct-gap semiconductors with a probe $\hbar\omega_a$ near the ND-2PA resonance. In ZnO, with $\hbar\omega_b$ at 16% of the bandgap, more than one order-of-magnitude enhancement of $n_2(\omega_a; \omega_b)$ over its zero-frequency limit is measured. In CdS, the sign change of $n_2(\omega_a; \omega_b)$ near the bandgap is also resolved. We found good agreement

Optics EXPRESS

between experimental results and our earlier theoretical predictions using nonlinear Kramers-Kronig relations [20–23,25], in both nondegenerate enhancement and spectral dispersion shapes of n_2. We therefore confirm the theory over an extremely large range of photon energy ratios, allowing predictions of the best operating wavelengths of semiconductor devices engineered to use cross-phase modulation.

Based on time-wavelength mapping of a linearly up-chirped probe pulse, we also demonstrate the anomalously dispersive behavior of extremely nondegenerate $n_2(\omega_a; \omega_b)$ near the bandgap in ZnO, which rapidly switches sign from the enhanced positive n_2 to a large negative value over a very narrow spectral range. This strongly dispersive NLR has potential to provide not only large but ultrafast modulation of a femtosecond pulse with bandwidth centered near the zero-crossing frequency to enable new applications such as nonlinear pulse shaping.

This enhancement of NLR also suggests the possibility of all-optical switching based on the nondegenerate Kerr effect. A larger $n_2(\omega_a; \omega_b)$ significantly reduces the switching energy for the required phase changes for all AOS devices. Also, the magnitude, sign, and dispersion of NLR can be significantly tailored with nondegenerate beams by selecting the appropriate excitation wavelength, which can lead to advantages over its degenerate counterpart. Operating in a nondegenerate scheme with a control beam at a (mid-) infrared wavelength, we can essentially avoid 2PA in the signal beam, leaving a relatively smaller nondegenerate 3PA as the dominant nonlinear loss, resulting in a larger FOM_{3PA}. Approximately 340 × improvement of the FOM_{3PA} over the degenerate case at the same signal wavelength has been measured in ZnSe when using < 1 GW/cm^2 switching irradiance.

Funding

Air Force Office of Scientific Research (MURI grant FA9550-10-1-0558); National Science Foundation (NSF) (ECCS-1202471 and ECCS-1229563); Army Research Laboratory (W911NF-15-2-0090).